The American Journal of Human Genetics

Supplemental Data

DCDC2 Mutations Cause a Renal-Hepatic Ciliopathy by Disrupting Wnt Signaling

Markus Schueler, Daniela A. Braun, Gayathri Chandrasekar, Heon Yung Gee, Timothy D. Klasson, Jan Halbritter, Andrea Bieder, Jonathan D. Porath, Rannar Airik, Weibin Zhou, Joseph J. LoTurco, Alicia Che, Edgar A. Otto, Detlef Böckenhauer, Neil J. Sebire, Tomas Honzik, Peter C. Harris, Sarah J. Koon, Meral Gunay-Aygun, Sophie Saunier, Klaus Zerres, Nadina Ortiz Bruechle, Joost P.H. Drenth, Laurence Pelletier, Isabel Tapia Pắez, Richard P. Lifton, Rachel H. Giles, Juha Kere, and Friedhelm Hildebrandt

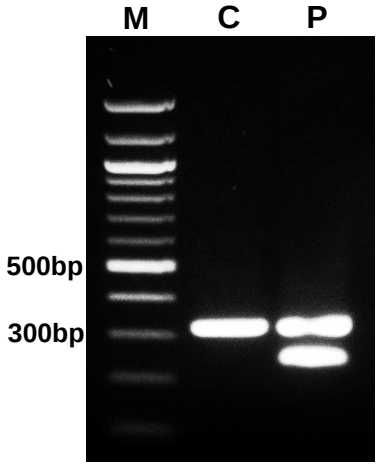

Figure S1. RT-PCR in individual A4435-21 with the c.349-2A>G mutation results in skipping of exon 4.

RT-PCR was performed on cDNA from white blood cells of A4435-21 (P) and healthy control (C) using primers 2F and 5R (see **Fig. 1C**) flanking exon 4. For healthy control a PCR product with the expected size of 323 bp was observed. In contrast, the RT-PCR of the affected individual yielded an additional PCR product of 246 bp, confirming that the detected heterozygous obligatory splice mutation c.349-2A>G results in skipping of exon 4 of *DCDC2*. Both PCR products were Sanger sequenced confirming missplicing of the *DCDC2* transcript (**Fig. 1F**). M, Marker 100 bp ladder.

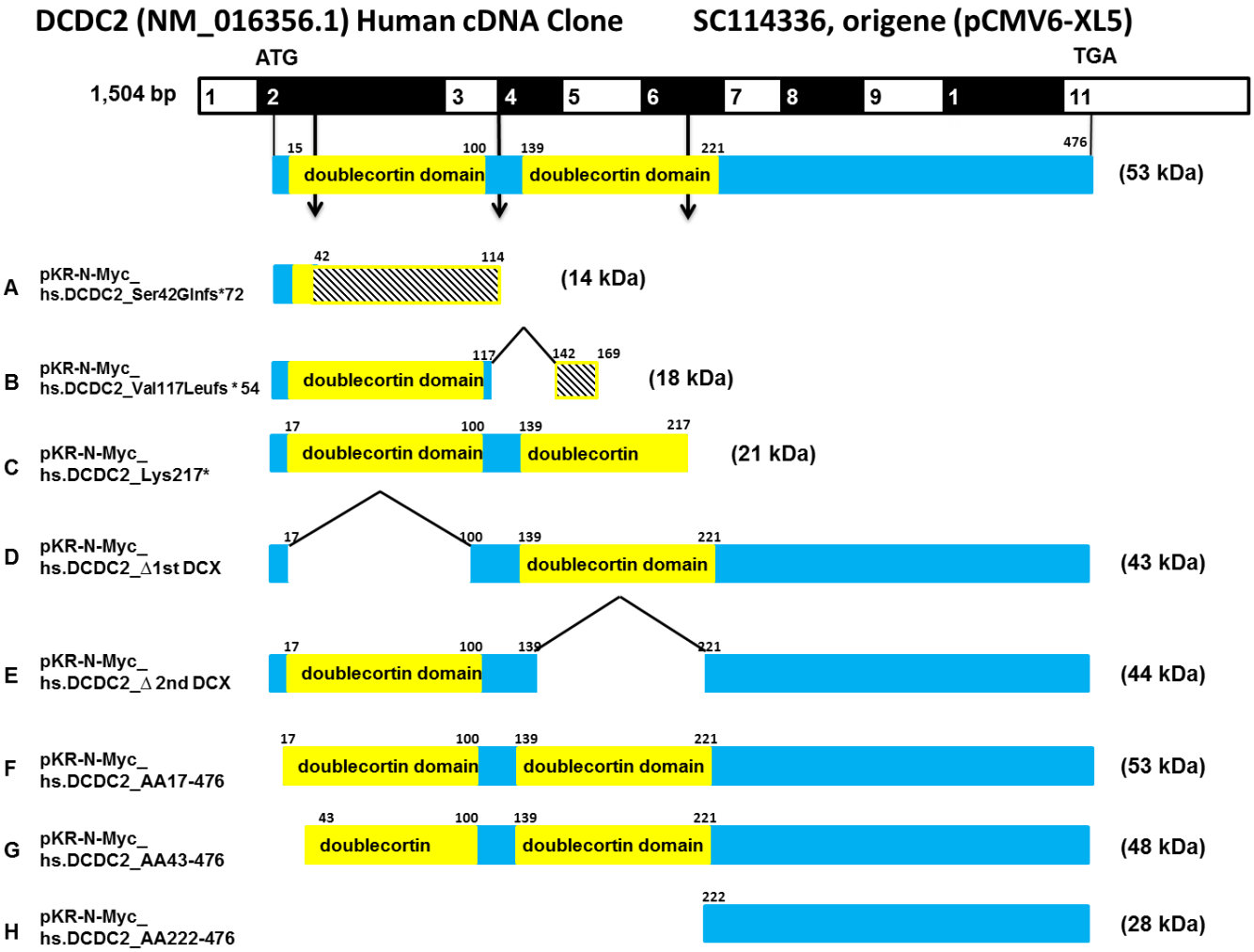

Figure S2. Domain structure of human mutations and artificial constructs in *DCDC2* .

(A) The most 5' terminal mutation causes a frameshift after 42 amino acids abrogating both doublecortin (DCX) domains.

(B) The splice site mutation causes skipping of exon 4 and a frameshift at amino acid 117 resulting in a protein truncation.

(C) The most 3' terminal mutation causes a protein truncation after 217 amino acids, resulting in a protein product that contains one complete and one partial DCX domain.

(D) An artificial construct lacking the 1st DCX domain.

(E) An artificial construct lacking the 2nd DCX domain.

(F) An artificial construct that lacks the region N terminal of the first DCX domain (first 17 amino acids).

(G) An artificial construct that lacks the first 42 amino acids that are preserved in the shortest human mutation.

(H) An artificial construct that lacks both DCX domains and contains amino acid 222 - 476 only.

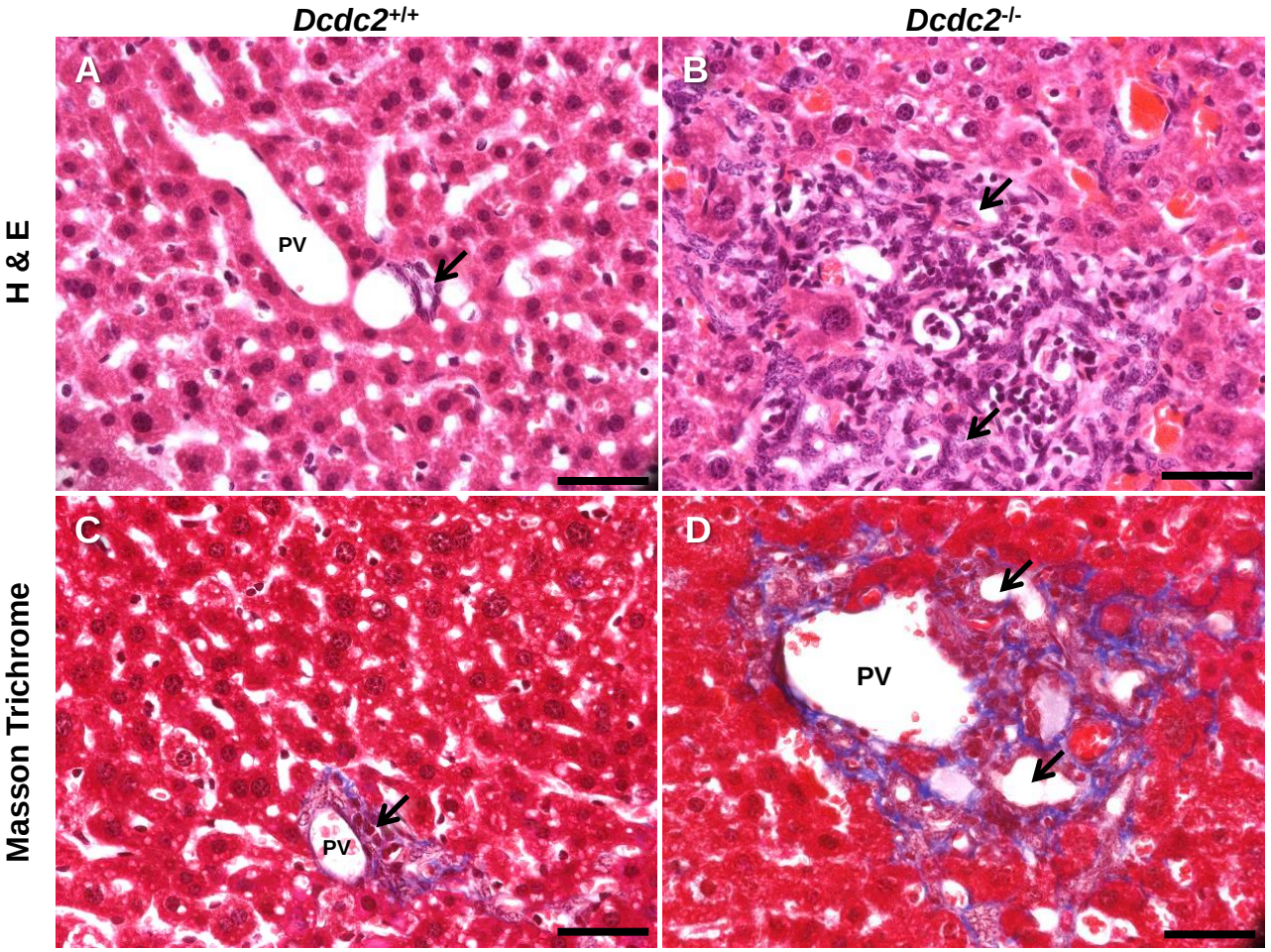

E

	Number of periportal fields with collagen deposition upon Masson Trichrome staining[1]		
Grade	**0, I**	**II, III**	**n periportal fields/animal**
***Dcdc2*$^{+/+}$ 11 months**	**7 (77.7%)**	**2 (22.2%)**	**9**
***Dcdc2*$^{-/-}$ 11 months**	**3 (27.2%)**	**8 (72.7%)**	**11**
n periportal fields	**10**	**10**	**20**

X^2=5.051 (p<0.05, 1 tailed)

[1] All periportal fields of 3 different sections from 3 different lobes per animal were evaluated.

Figure S3. Liver histology reveals periportal liver fibrosis in *Dcdc2*$^{-/-}$ mice.
Hematoxylin and eosin staining (H & E) of 11 months old *Dcdc2*$^{+/+}$ (**A**), and 11 months old *Dcdc2*$^{-/-}$ mice demonstrate biliary duct proliferation in *Dcdc2*$^{-/-}$ animals (**B**)
(**C**, **D**) Masson Trichrome staining (MTS) shows when compared to wild type control (**C**) extensive collagen deposition around the portal tracts in *Dcdc2*$^{-/-}$ animals (**D**).
(**E**) Table quantitates degree of collagen deposition within periportal fields of three different liver lobes per animal from blinded evaluation of MTS. Grades 0/I indicate presence of few collagen fibers surrounding the vessel walls and within the extracellular matrix (**C**). Grades II/III represent periportal fields with an increased deposition of collagen fibers along the circumferences of the bile ducts spreading into the liver parenchyma (**D**). Similar data were obtained from another *Dcdc2*$^{-/-}$ animal (data not shown).
Note the increased number of periportal fields ranked II or III grade in the *Dcdc2*$^{-/-}$ mice.
PV: branch of portal vein; arrow: bile duct; Scale bar: 500 µm.

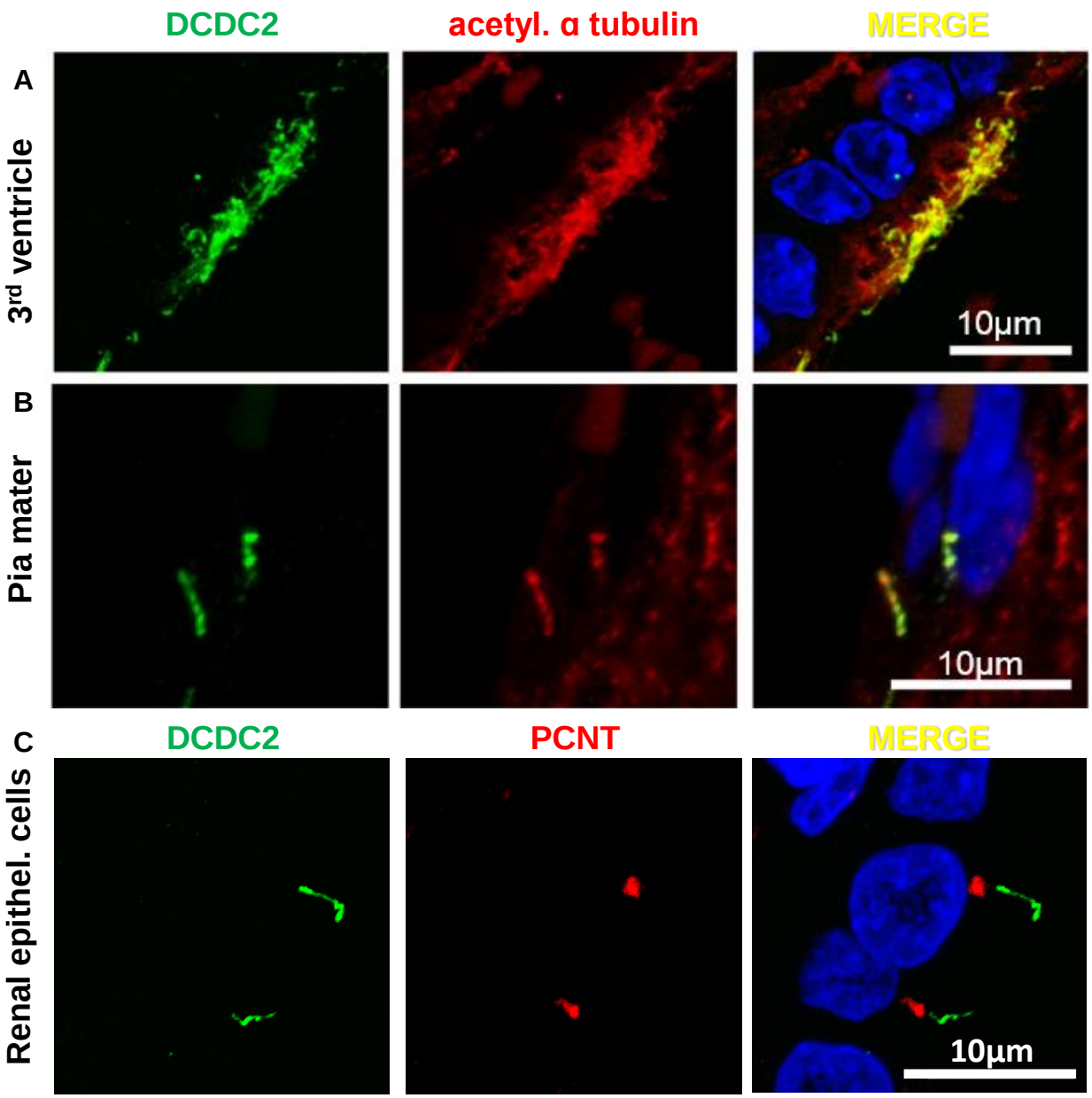

Figure S4. DCDC2 decorates the axoneme of primary cilia in ependymal cells of the third brain ventricle, and of the cranial pia mater in mice as well as of human renal epithelial cells, but does not localize to the basal body.

(**A**) DCDC2 co-localizes with acetylated-α-tubulin at the ciliary axoneme of ependymal cells in the third ventricle of the brain, (**B**) of cells in the cranial pia mater. (**C**) Axonemal localization excludes the basal body (marker PCNT) as shown in human renal epithelial cells. Coronal brain of FVB/N mice (male, 3 mo old) were fixed with 4% PFA/PBS by immersion, paraffin-embedded and sectioned. Tissue sections were blocked with 5% horse serum/0.05% PBS-Triton X-100 and immuno-stained with anti-DCDC2 antibody (green, Santa Cruz), anti-acetylated-α-tubulin antibody (red, Sigma) or anti-PCNT antibody (red, Atlas antibodies) and DRAQ5 to label DNA (blue).

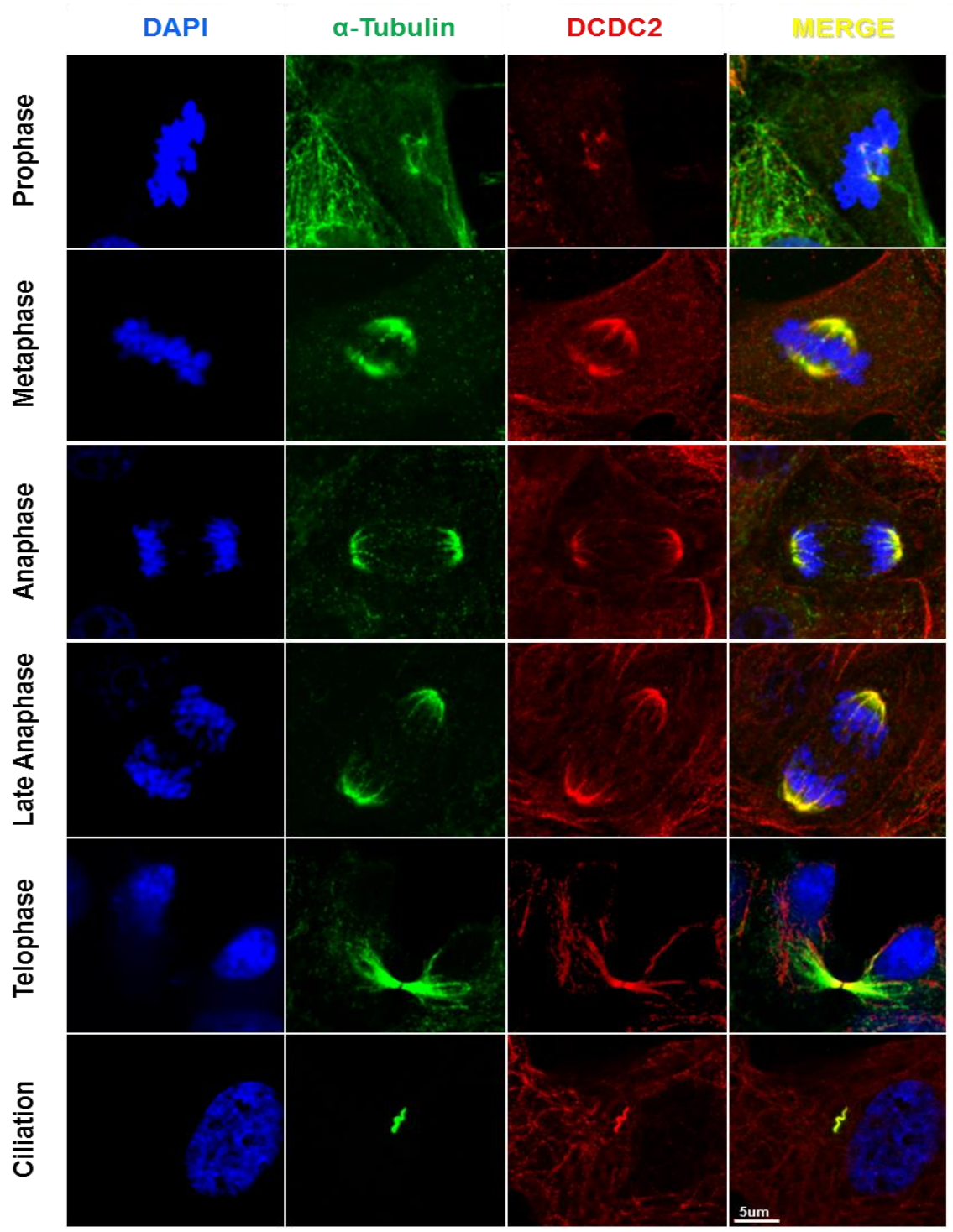

Figure S5. DCDC2 colocalizes with acetylated α-tubulin to mitotic spindle fibers and the ciliary axoneme.

DCDC2 localizes to the mitotic spindle throughout the phases of mitosis, sparing the spindle poles and the interpolar spindle fibers in metaphase. Upon serum starvation DCDC2 decorates the ciliary axoneme. In telophase it labels the abscission structure.

Cells were seeded at low density onto coverslips. For cell cycle images MDCK-II cells were grown to ~80% confluency. For ciliation images hTERT-RPE were serum starved for 48 hrs. Cells were fixed (4% PFA), permeabilized (0.1% SDS) and immuno stained with mouse anti-acetylated-α-tubulin antibody (green, abcam), rabbit anti-DCDC2 antibody (red, abcam), DAPI to label DNA (blue).

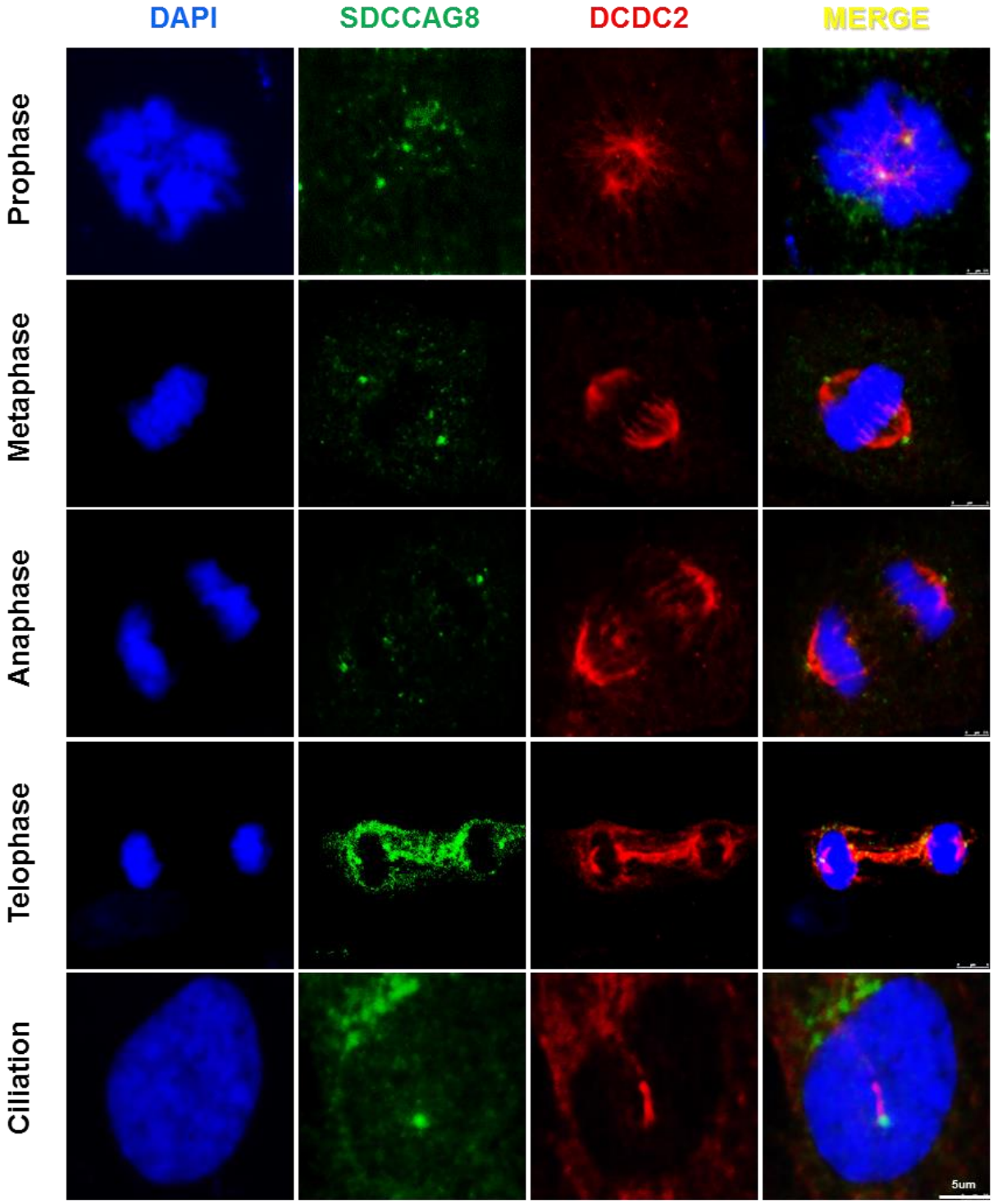

Figure S6. In contrast to the established ciliopathy protein SDCCAG8, which stains spindle poles and basal bodies, DCDC2 stains spindle microtubules and the ciliary axoneme.

hTERT-RPE1 were seeded onto coverslips, grown to confluency and serum-starved for 36 hrs. Cells were fixed (4% PFA), permeabilized (0.1% SDS), and immuno-stained with anti-SDCCAG8 (green). Costaining was performed using an anti-DCDC2 antibody (red, abcam) and DAPI to label DNA (blue).

Note that DCDC2 stains spindle fibers (metaphase and anaphase) and the entire axoneme of primary cilia ('ciliation'), but does not colocalize with the centrosomal ciliopathy protein SDCCAG8 to spindle poles or basal bodies.

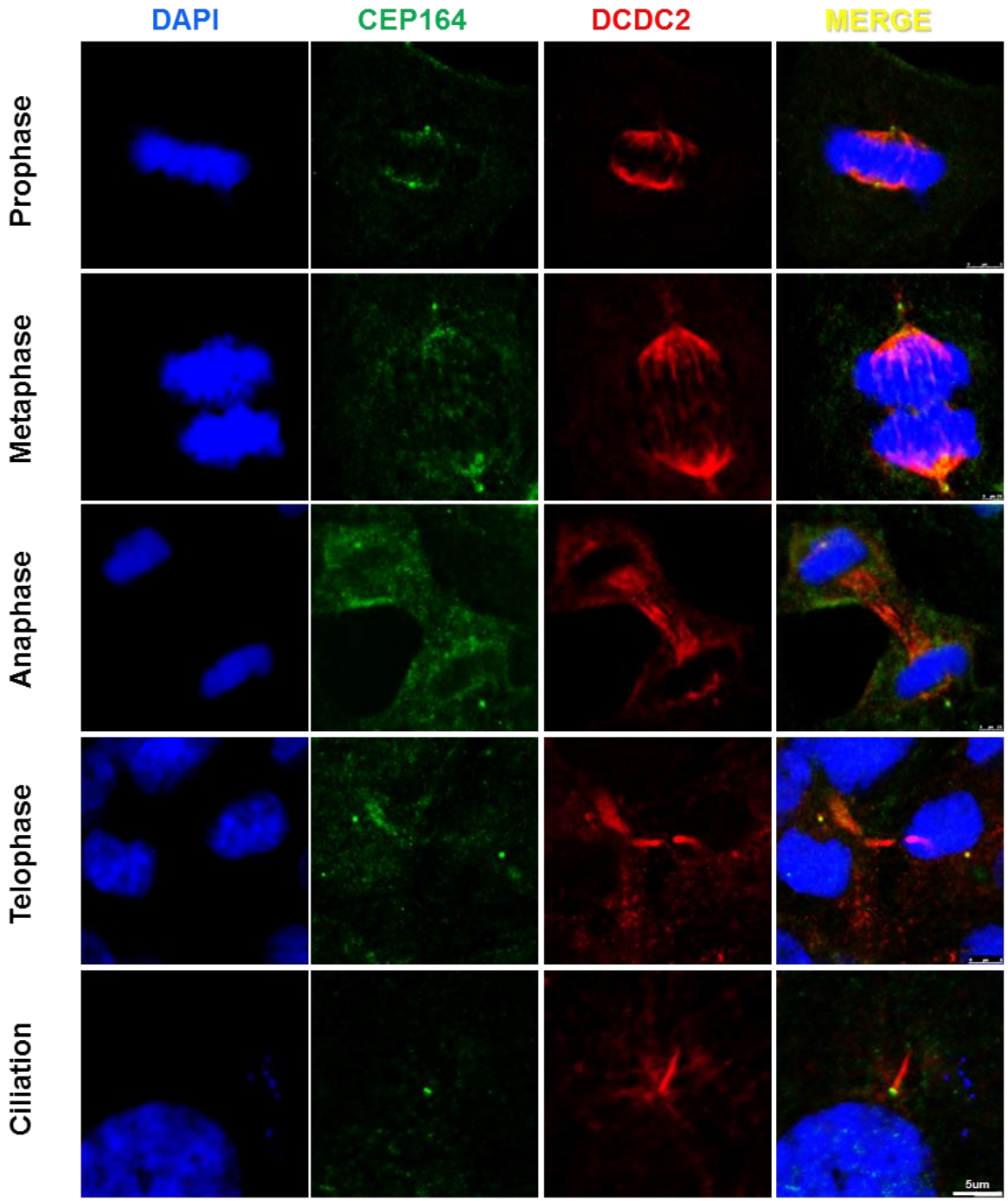

Figure S7. In contrast to the established ciliopathy protein CEP164, which stains spindle poles and basal bodies, DCDC2 stains spindle microtubules and the ciliary axoneme.

hTERT-RPE1 were treated as described before (**Suppl. Fig. 6**) and immuno-stained with anti-CEP164 antibody (green). Costaining was performed using an anti-DCDC2 antibody (red, abcam) and DAPI to label DNA (blue).

Note that DCDC2 stains spindle fibers (metaphase and anaphase) and the entire axoneme of primary cilia, but does not colocalize with the centrosomal ciliopathy protein CEP164 to spindle poles or basal bodies.

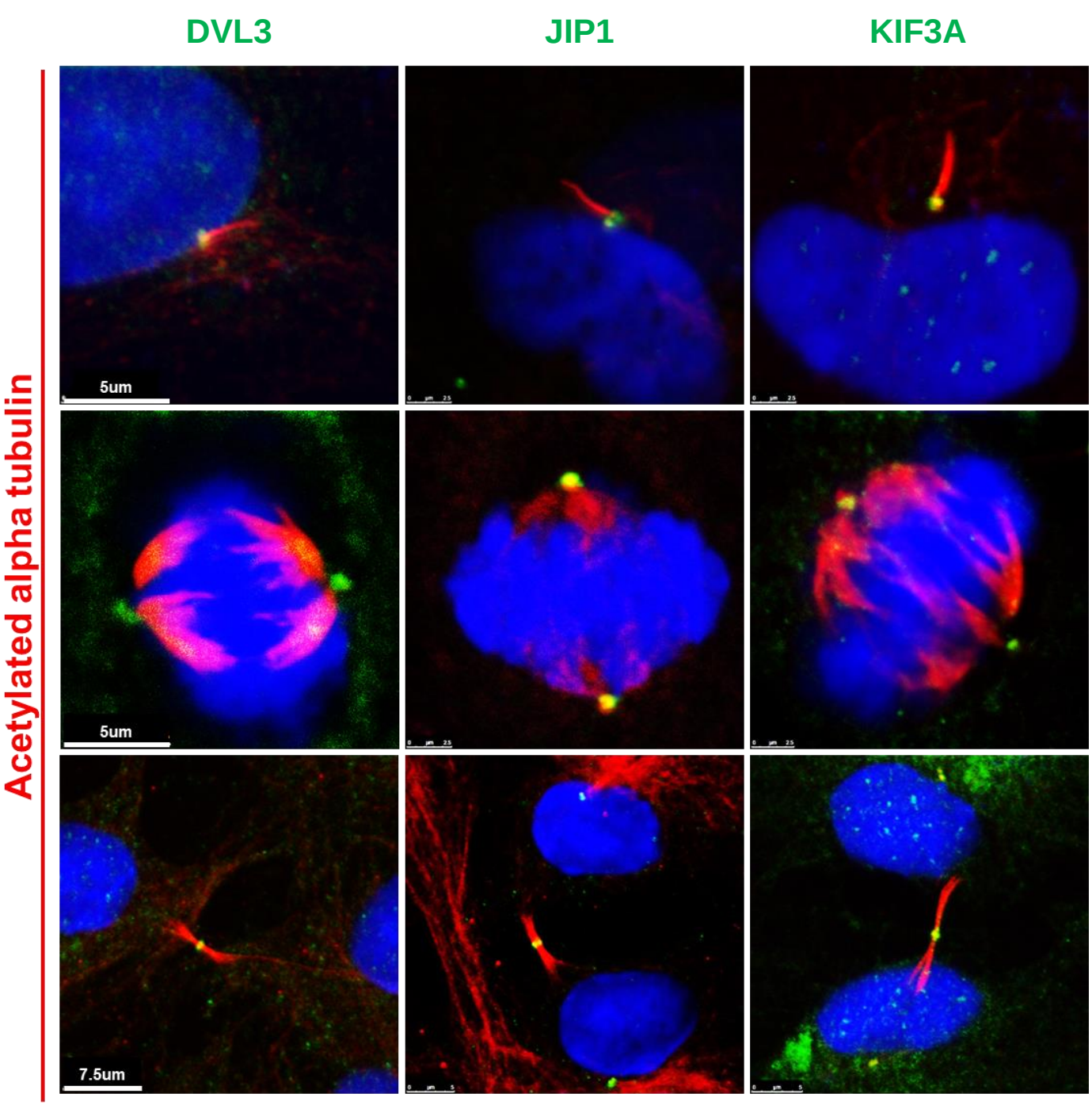

Figure S8. Interaction partners of DCDC2 show a similar localization pattern throughout cell cycle.

The localization pattern of the interacting proteins DVL3, JIP1, and KIF3A was analyzed in comparison to acetylated alpha tubulin in ciliated cells, in metaphase and cytokinesis. All three proteins colocalize to the basal body, the mitotic spindle poles and the midbody.

hTERT-RPE1 cells were seeded on coverglasses, grown to confluency and serum starved for 48 hrs to induce ciliation. Fixation and permeabilization was done using aceton, DAPI was used to stain nuclei.

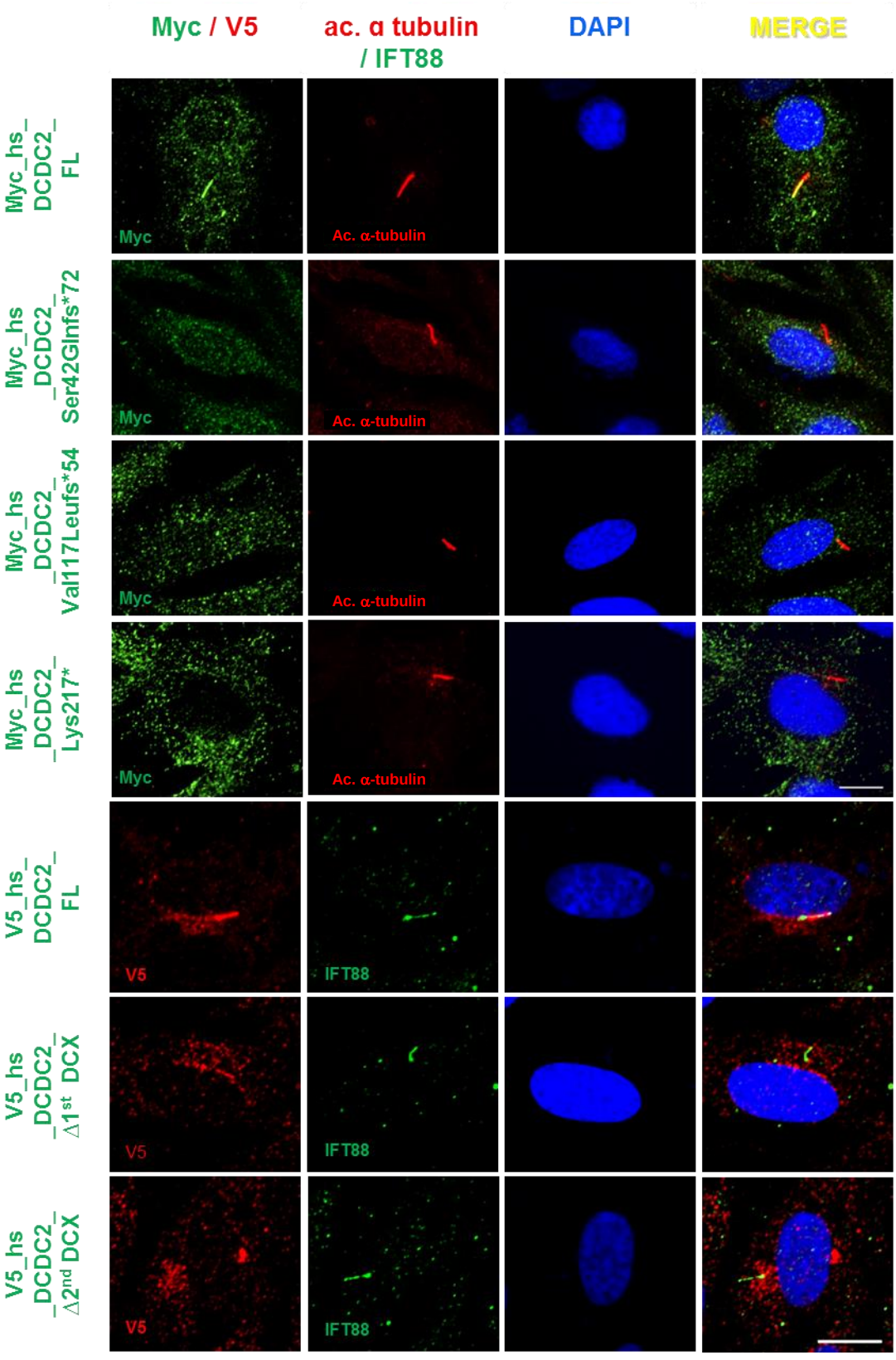

Figure S9. Wildtype but not mutant DCDC2 localize to the primary cilia in RPE1-cells.

RPE1 cells transfected with wildtype human DCDC2 show localization to the primary cilium. The localization is abrogated in all mutations found in humans with ciliopathies (rows 2-4) and in artificial constructs, in which either of the two doublecortin domains are missing (rows 5 and 7). DNA was labeled with DRAQ5 (blue). Scale bar 10µm.

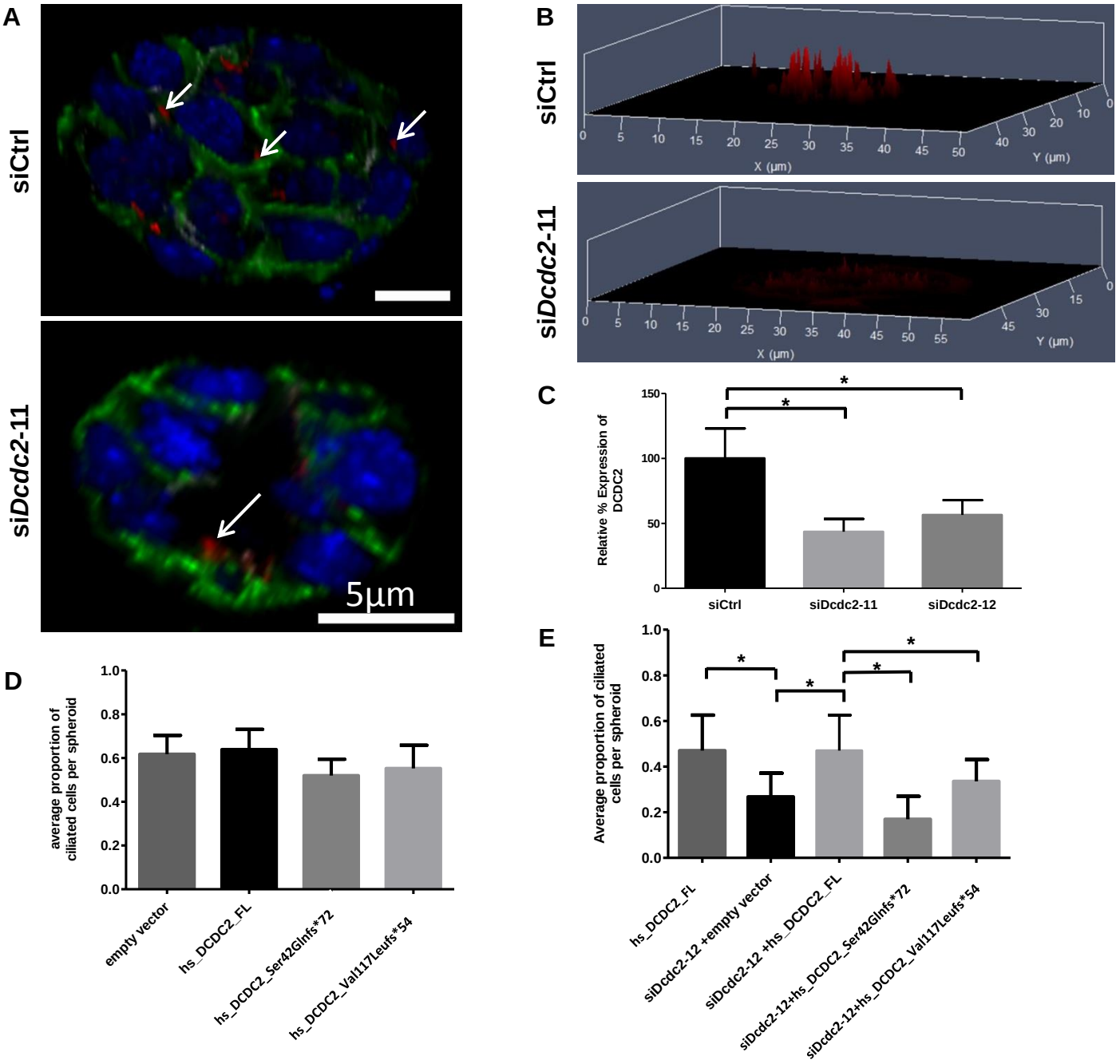

Figure S10. 3D representation of cilia loss after *Dcdc2* knockdown in IMCD3 cells.

*Dcdc*2 knockdown causes a ciliation defect, which is not rescued by *DCDC2* mutants detected in NPHP-RC, but is rescued by overexpression of full length human *DCDC2* (hsDCDC2_FL).

(A) 3D renderings of partial Z-stacks of IMCD3 spheroids show a loss of ciliation after *Dcdc2* knockdown (settings are identical between conditions). Acetylated tubulin (red, marked with arrows) indicates the presence of cilia.

(B) 2.5D surface renderings of Z-stacks demonstrate that the intensity of acetylated tubulin staining in the lumen of spheroids noticeably decreases after *Dcdc2* knockdown.

(C) qPCR validation of the knockdown efficiency of siRNA *DCDC2*-11 *and DCDC2*-12 in IMCD3 cells.

(D) Average proportion of ciliated IMCD3 cells per spheroid for overexpression of full length human *DCDC2,* empty vector, and three mutants found in humans with ciliopathies, showing no effect on ciliary frequency.

(E) Average proportion of ciliated IMCD3 cells per spheroid upon knockdown with a second siRNA (si*Dcdc2*-12A) as validation of the observed ciliogenesis defect and allelic reconstitution.

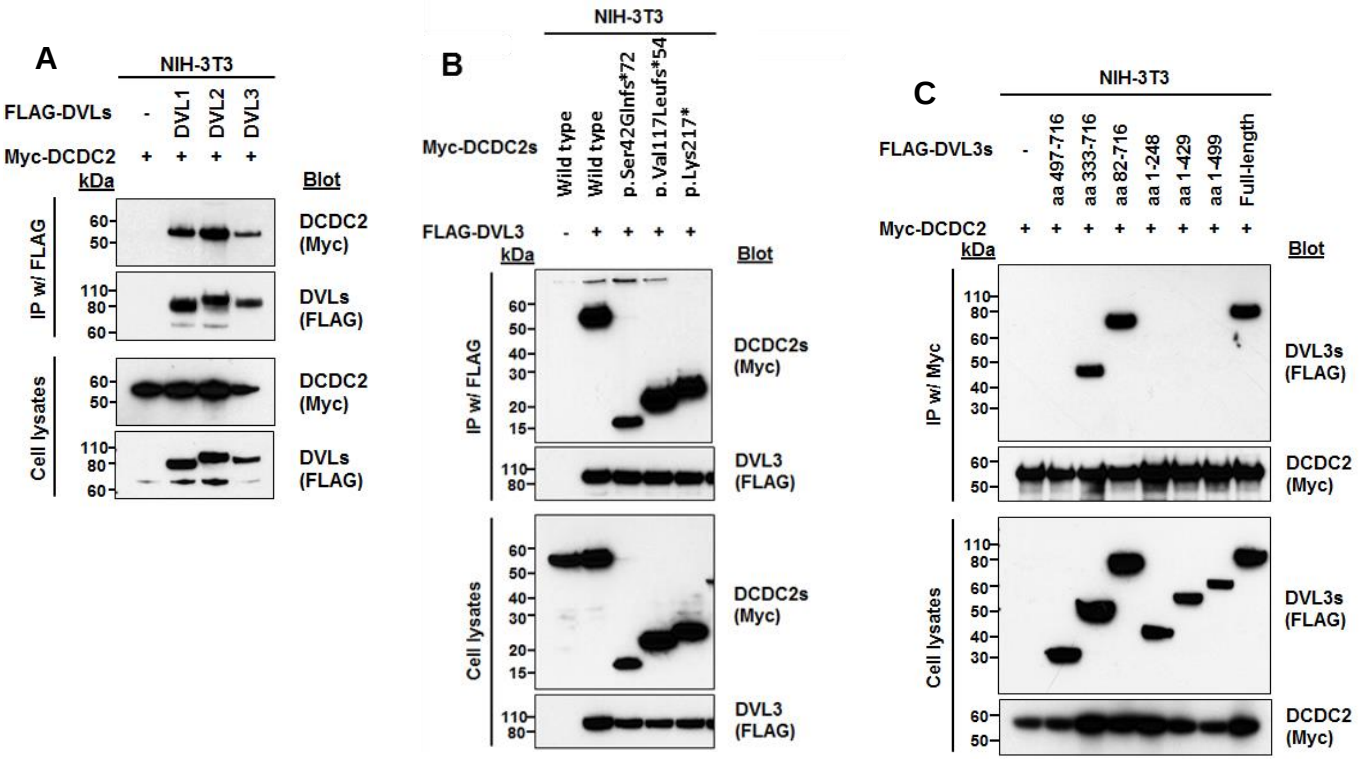

Fig S11. DCDC2 interacts with dishevelled (DVL). The human mutations do not abrogate the interaction.

(A) Co-immunoprecipitation with Myc tagged DCDC2 and Flag tagged Dvl shows that DCDC2 interacts with DVLs (DVL1, DVL2 and DVL3) when transiently overexpressed in NIH-3T3 cells.

(B) None of the three human mutations abrogate this interaction.

(C) The partial DVL3 clone (497-716aa) and the C-terminal DVL3 deletion clones (1-248 aa, 1-429 aa and 1-499 clones) show loss of interaction with DCDC2 by immunoprecipitation using a Myc-tag of DCDC2. Therefore, the C-terminus of DVL3, which includes a DEP (Dishevelled, Egl-10 and Pleckstrin) domain, is necessary for the interaction with DCDC2.

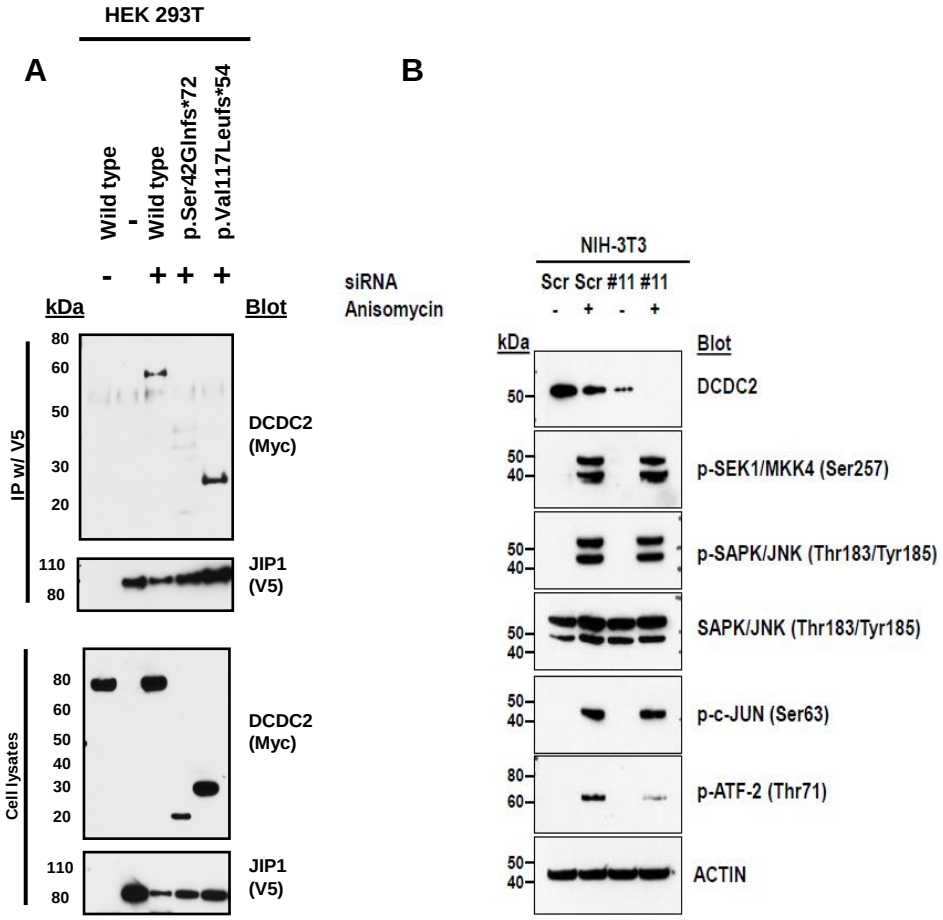

Figure S12. DCDC2 interacts with JIP1.

(**A**) Protein-protein interaction between DCDC2 wild-type (WT) and JIP1 full length (lane 3), and the effect of the two *DCDC2* mutations p.Ser42Glnfs*72 and p.Val117Leufs*54 on the interaction with JIP1 (lanes 4 and 5). Note that while p.Val117Leufs*54 still interacts with JIP1 (lane 5), p.Ser42Glnfs*72 abrogates the interaction between DCDC2 and JIP1 (lane 4). (For DCDC2 constructs see **Suppl. Fig. 2**)

(**B**) Knockdown (#11) of *Dcdc2* in NIH-3T3 cells does not affect the JNK pathway activation. Scrambled (Scr) siRNA was used for negative control. Phosphorylation of the JNK downstream target c-Jun and ATF2 was used as the read-out. Anisomycin (50 μg/ml) shows pharmacological activation of the pathway and increased phosphorylation of c-Jun and ATF2.

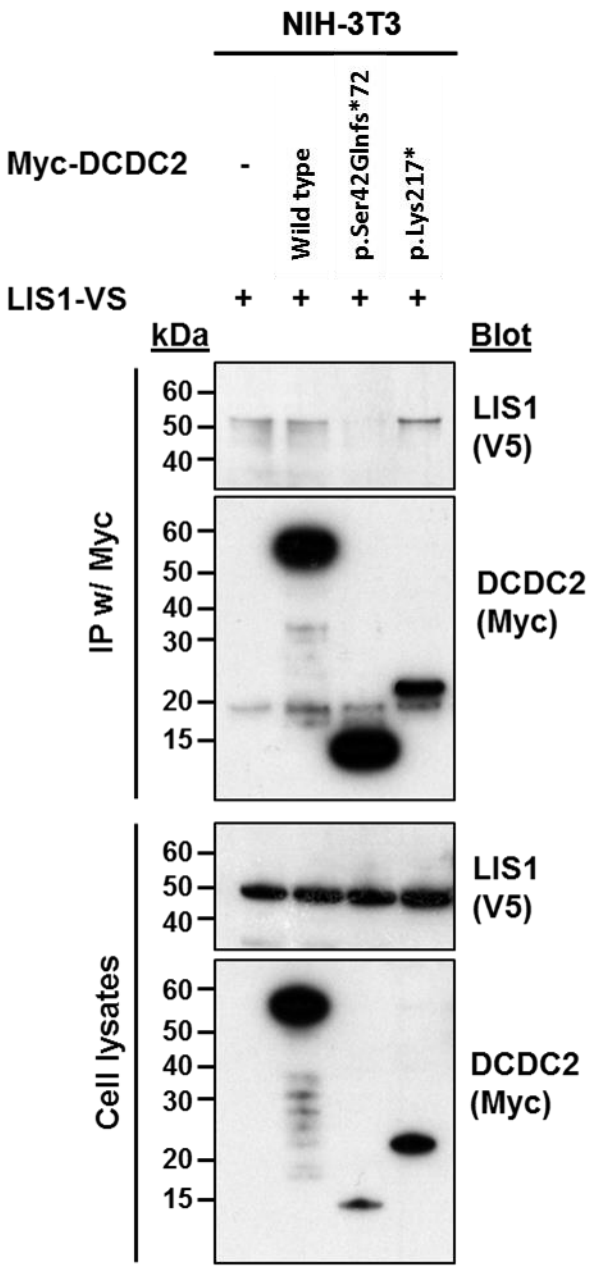

Figure S13. DCDC2 does not interact with LIS1.
C-terminally V5-tagged *LIS1* and N-terminally Myc-tagged *DCDC2* constructs were transfected into NIH-3T3 cells and coimmunoprecipitated with a Myc antibody. There was no protein-protein interaction between LIS1 and DCDC2. Images are representative of two experiments. IP denotes immunoprecipitaiton.

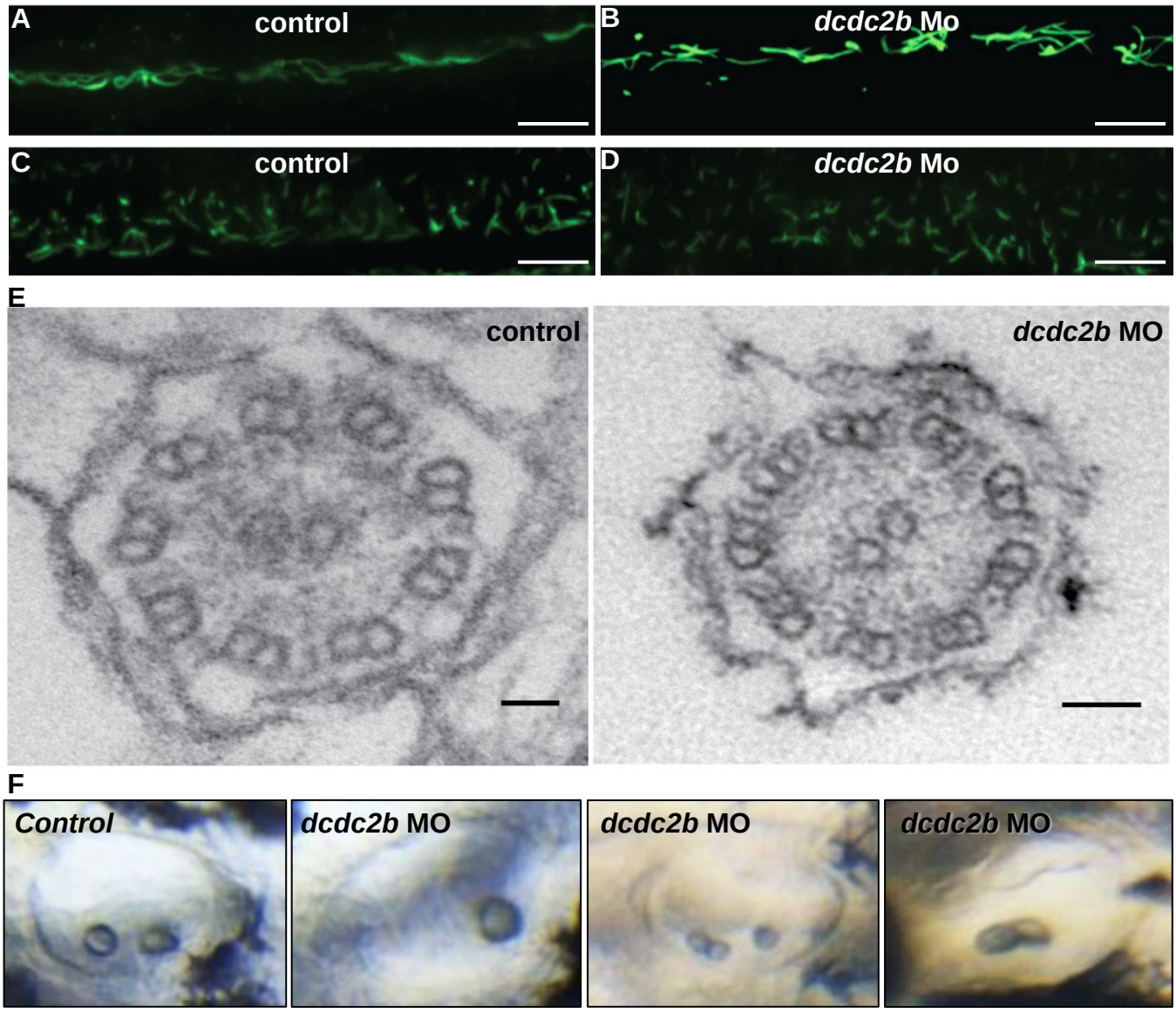

Figure S14. Knockdown of *dcdc2b* does not alter cilia length in zebrafish kidney and spinal cord nor ultrastructure of pronephric cilia.

Pronephric cilia of control and of *dcdc2b* morphant zebrafish embryos were immunostained one day post fertilization with anti-acetylated α-tubulin antibody**.**

(A/B) Cilia (green) in pronephric kidney of *dcdc2b* MO (right panel) do not show a difference in length compared to uninjected control (right panel).

(C/D) Spinal cord cilia length did not differ in length between conditions of control(left panel) and MO knockdown (right panel). Scale bar: 50 um

(E) The ultrastructure of motile cilia in pronephric kidney does not differ between conditions of control (left panel, scale bar: 200 nm) and *dcdc2b* MO knockdown (right panel, scale bar 100 nm).

(F) Representative images of *dcdc2b* morphants (AUGMo) at 3 dpf show variable otolith numbers ranging from 1-3 (64/147 = 43.5%), whereas control display normal pattern of two otoliths (5/114 = 4.4%).

Table S1. Filtering process for variants from normal reference sequence (VRS) following WES in one sibling from family A3547-22 affected with NPHP-RC.

FAMILY	A3547
[a]AFFECTED individual SENT FOR WES	A3547-22
Consanguinity	Yes
[b]# of homozygosity peaks	8
Cumulative Homozygosity by descent[c] [Mb]	124
[c]Hypothesis from mapping: homozygous (H), heterozygous (h)	H
Total sequence reads (Mill.)	454
Matched Reads	98.1%
Total DIPs	10,259
Exonic DIPs	249
% exonic / total DIPs	2.40%
DIPs in linked region	16
DIPs after inspection and not SNP138 (>1% MAF)	0
Sanger confirmation / Segregation	0
Total SNPs	29,402
Exonic SNPs	1,674
% exonic / total SNPs	5.60%
SNPs in linked region	139
SNPs after inspection and not SNP138 (>1% MAF)	5
[d]Sanger confirmation / Segregation	1
gene with causative mutation	*DCDC2*
Mutation effect on gene product	K217* (H)

[a]see Table 1

[b]see Fig. 1

[c]evaluation for homozygous variants was done in regions of homozygosity by descent for 1 affected individual

[d]red numbers denote number of filtered-down variant(s) that contained the gene with disease causing mutation

DIP, deletion/insertion polymorphism; SNPs, single nucleotide polymorphism; NPHP-RC, Nephronophthisis-related ciliopathies

Table S2. Final remaining variants after filtering process

DCDC2 truncating mutation is highlighted in yellow to indicate ranking as most likely disease causing.

Diagnosis: NPHP-RC

Total homozyg. [Mb]: 124041201
Hom. peaks: 8
Other captures: No

Poly 2
0 - 0.7
0.7 - 0.9
0.9 - 1.0

individual	Gene	hg19 pos.	Nt change >	Accession #	AA change p.	Conservation							Mut Taster	SIFT	Poly2	EVS
						Mm	Gg	Xt	Dr	Ci	Ce	Dm				
A3547-22	*DCDC2*	chr6:24291215	T>A	NM_001195610.1	p.K217*											no
	TATDN3	chr1:212981117	C>T	NM_001042552.2	p.P176L	P	P	P	P	S	P	A	Pol	Del	0.015	no
	BIRC6	chr2:32667182	G>C	NM_016252.3	p.V1332L	L	L	T	L	S	-	-	DC	Del	0.9	no
	CCDC66	chr3:56650056	>CTC	NM_001141947.1	p.S606delinsSP	S	-	-	Q	-	-	-				A1A1=76/A1R=525/RR=1201
	CLDN16	chr3:190106073	G>C	NM_006580.3	p.R55S	Q	-	-	-				Pol	Tol	0.01	no

Table S3: Primer

Primer	Primer Sequence Forward	Primer Sequence Reverse	Size
DCDC2, Exon2_1	CGAAGCTGGACACCTTCTT	CTCTTTCACCTGTGGATTCG	271bp
DCDC2, Exon 2_2	ATCTGCATTTCTTCATATCAACC	CCTTCTACGCGGGGC	287bp
DCDC2, Exon3	GAGAACTCATCAAAGTAGAATGCC	AACTCTTATTGTTTGTTTGTTTTTTCC	188bp
DCDC2, Exon4	GCAAGGTTTTAACAAAGGCAC	CAAACCAAAAGGAAACCACC	262bp
DCDC2, Exon5	TCAACAATTCAAAAACTCCTCC	TGGTTTCCTTTTGGTTTGG	257bp
DCDC2, Exon6_1	TGGTGGTCAGCAAAAGACC	GAAGGAAAACTTGTTGAGAGTGG	209bp
DCDC2, Exon6_2	GCAGTTTCTTAAACTTATCTCTGCC	GGCATCTATAATGCAATAATGAGG	270bp
DCDC2, Exon 7	ACAGTTGACTTCCAGGTGGG	GAAGCCCAAAGGACAGTCTC	222bp
DCDC2, Exon8_1	GGCCCAGAGAAACAATGG	GGTCTAATACTTTGCCATTTAGGG	259bp
DCDC2, Exon8_2	AATTCACGTCTTCTTTTTTCCC	ACCCTTTTGCCTCCAGG	275bp
DCDC2, Exon9	CCTTAGAGGGTTTAATTCATACAGG	CAGCATTCAGCCACACG	278bp
DCDC2, Exon10_1	CATTCACATAAGCAAGCAAAAGC	TGACCTTGAAGAGGAAGGAGG	248bp
DCDC2, Exon 10_2	CTCACCATTCTCCTCATC	GCAGTGGAAATGTTCTGTTATGC	279bp
DCDC2, Exon11	TGCTTATCTTTCAAGTATGATAACCC	TTACCTTTGTGAACCAAACAGC	229bp
DCDC2, cDNA exon2	CGGAAGCTAGACCAGATCCA		
DCDC2, cDNA exon5		CCGCTCCTCAGAGTGATTTT	
Dcdc2b ATG MO	CCGGTGGATGCCATGACTTTTCAGT		
Dcdc2b Splice MO	GCCATGACCTTAAATTAATCACATT		
siRNA murine dcdc2	CCAGAUGCCUAAAGCGUUA		
siRNA murine dcdc2	GAUGCAGGGCAGCGCUUUA		